Molecular Cell, Volume *80*

Supplemental Information

A Selective Autophagy Pathway for Phase-Separated Endocytic Protein Deposits

Florian Wilfling, Chia-Wei Lee, Philipp S. Erdmann, Yumei Zheng, Dawafuti Sherpa, Stefan Jentsch, Boris Pfander, Brenda A. Schulman, and Wolfgang Baumeister

SUPPLEMENTAL FIGURES AND FIGURE LEGENDS

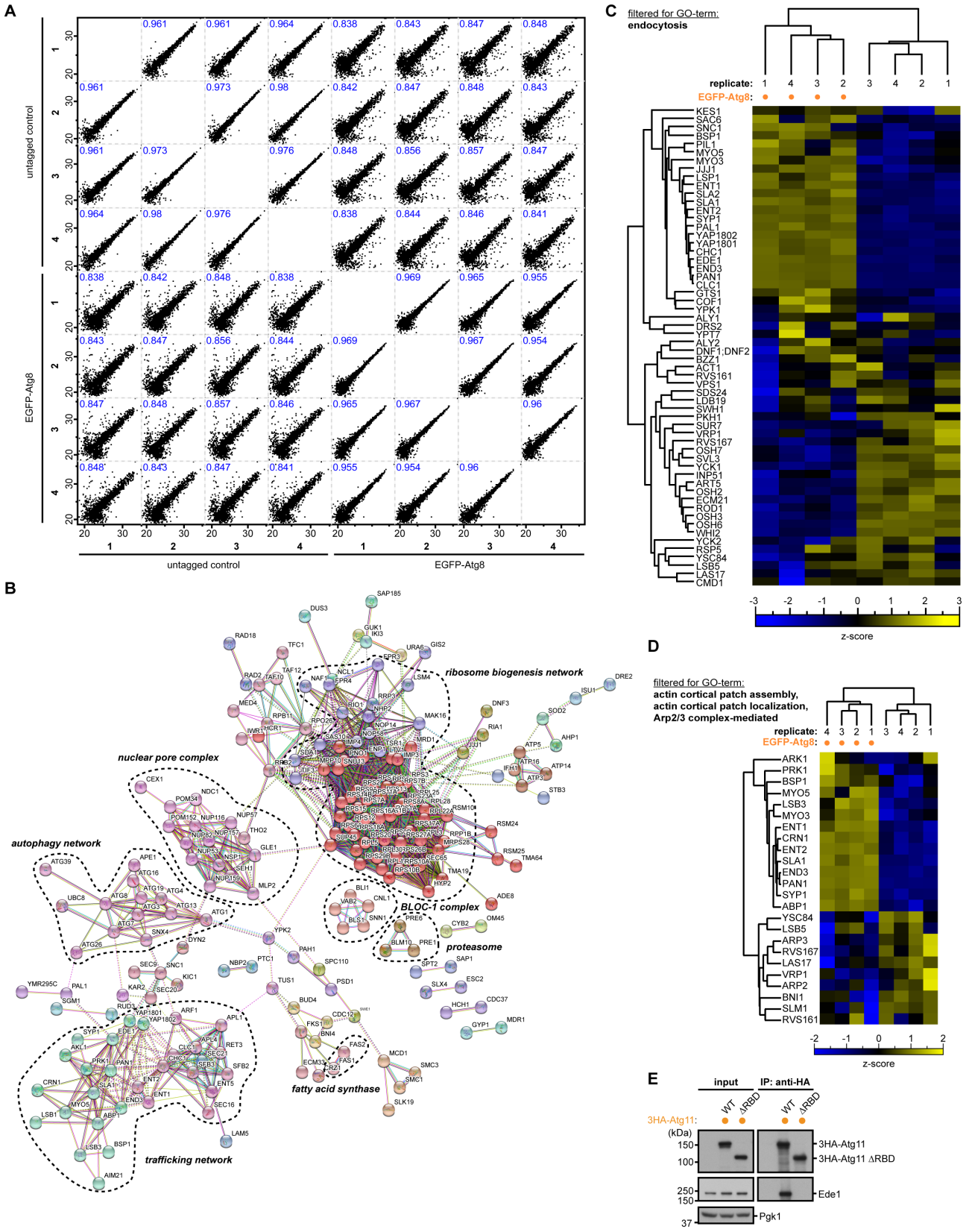

Figure S1. qMS Identified Components of Endocytic Machinery as Novel Atg8 Interactors, Related to Figure 1

(A) Multi scatter plot comparing all samples in relation to each other. The Pearson coefficient is indicated in each box with blue.

(B) STRING analysis of protein-protein interaction networks of the 225 specific EGFP-Atg8 interactors reveals binding of distinct complexes. Only proteins with at least one connection are shown.

(C-D) Hierarchical cluster analysis of Atg8 interactors filtered for GO-terms endocytosis or actin machinery. All EGFP-Atg8 specific interactors were filtered for GO-terms endocytosis (C) or Arp2/3 complex mediated actin nucleation, actin cortical patch assembly and actin cortical patch localization (D). Matching ANOVA-positive and FDR corrected hits are displayed by hierarchical clustering of the respective z-scores for each sample.

(E) Binding of Ede1 to the autophagic scaffold protein Atg11 *in vivo* depends on the presence of the fourth coiled coil domain. Atg11 full length or ΔRBD (1-859 aa) expressed under the *ADH* promoter was 3HA-epitope-tagged, and its interaction with Ede1 was probed by co-immunoprecipitation and immunoblotting with anti-Ede1 antibody.

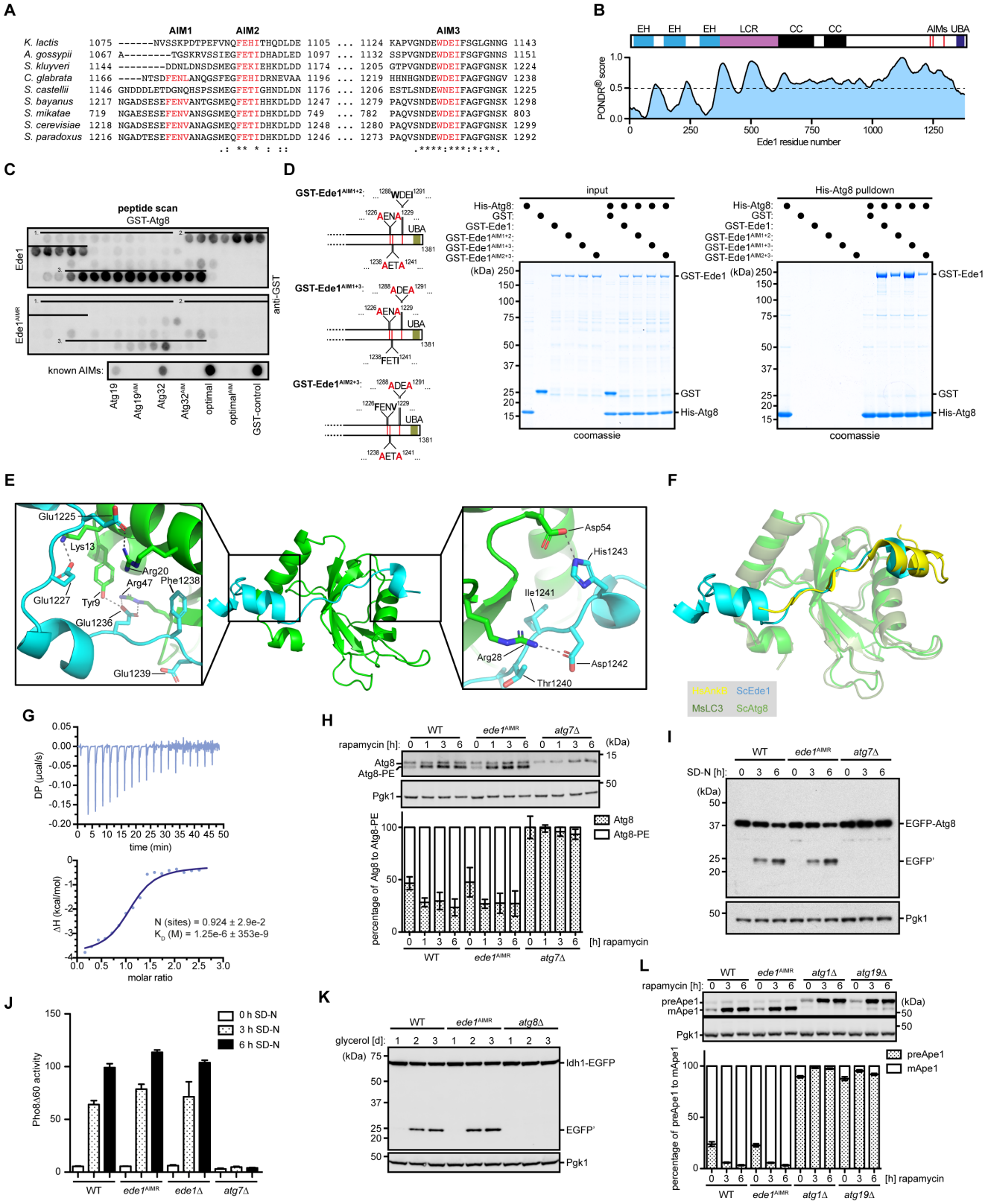
A
AIM1
AIM2
AIM3
K. lactis 1075 ------NVSSKPDTPEFVNQFEHITHQDLDE 1105 ... 1124 KAPVGNDEWDEIFSGLGNNG 1143
A. gossypii 1067 A---------TGSKRVSSIEGFETIDHADLED 1097 ... 1132 SSPVGNDEWDEIFSGFGNNS 1151
S. kluyveri 1144 ---------DDNLDNSDSMEGFEKIEHKDLDD 1174 ... 1205 GTPVGNDEWDEIFAGFGNSK 1224
C. glabrata 1166 ----NTSDFENLANQGSFEGFEHIDRNEVAA 1196 ... 1219 HHNHGNDEWDEIFAGFGNGV 1238
S. castellii 1146 GNDDDLETDGNQHSPSSMEGFETIGHNDLDN 1176 ... 1206 ESTLSNDEWNEIFAGFGNGK 1225
S. bayanus 1217 NGADSESEFENVANTGSMEQFETIHHKDLDD 1247 ... 1279 PAQVSNDEWDEIFAGFGNSK 1298
S. mikatae 719 NGAESESEFENVANSGSMEQFETIDHKDLDD 749 ... 782 PAQVSNDEWDEIFAGFGNSK 803
S. cerevisiae 1218 NGADSESEFENVANAGSMEQFETIDHKDLDD 1248 ... 1280 PAQVSNDEWDEIFAGFGNSK 1299
S. paradoxus 1216 NGADTESEFENVANAGSMEQFETIDHKDLDD 1246 ... 1273 PAQVSNDEWDEIFAGFGNSK 1292
B
EH EH EH LCR CC CC AIMs UBA
PONDR® score
Ede1 residue number
C
peptide scan
GST-Atg8
Ede1
Ede1AIMR
anti-GST
known AIMs:
Atg19
Atg19AIM
Atg32
Atg32AIM
optimal
optimalAIM
GST-control
D
GST-Ede1AIM1+2:
GST-Ede1AIM1+3:
GST-Ede1AIM2+3:
UBA
input
His-Atg8 pulldown
His-Atg8:
GST:
GST-Ede1:
GST-Ede1AIM1+2:
GST-Ede1AIM1+3:
GST-Ede1AIM2+3:
(kDa)
GST-Ede1
GST
His-Atg8
coomassie
E
Glu1225
Lys13
Arg20
Arg47
Phe1238
Glu1227
Tyr9
Glu1236
Glu1239
Asp54
His1243
Ile1241
Arg28
Asp1242
Thr1240
F
HsAnk8
ScEde1
MsLC3
ScAtg8
G
DP (µcal/s)
time (min)
ΔH (kcal/mol)
N (sites) = 0.924 ± 2.9e-2
K_D (M) = 1.25e-6 ± 353e-9
molar ratio
H
WT
ede1AIMR
atg7Δ
rapamycin [h]:
(kDa)
Atg8
Atg8-PE
Pgk1
percentage of Atg8 to Atg8-PE
[h] rapamycin
I
SD-N [h]:
EGFP-Atg8
EGFP'
Pgk1
J
0 h SD-N
3 h SD-N
6 h SD-N
Pho8Δ60 activity
WT
ede1AIMR
ede1Δ
atg7Δ
K
atg8Δ
glycerol [d]:
Idh1-EGFP
EGFP'
Pgk1
L
atg1Δ
atg19Δ
preApe1
mApe1
percentage of preApe1 to mApe1

Figure S2. Autophagy Pathways Are Unaffected in *ede1*^{AIMR} Mutant Strain, Related to Figures 2 and 3

(A) AIM2 and 3 are conserved among different yeast species as shown by multiple sequence alignment (https://www.ebi.ac.uk/Tools/msa/clustalo/).

(B) AIMs are located in the intrinsic disordered C-terminal region of Ede1. Output of intrinsic disorder prediction program PONDR (http://www.pondr.com) for Ede1, with schematic views of Ede1 structural elements. EH: Eps15-homology domain; LCR: low complexity region; CC: coiled-coil domain; UBA: ubiquitin-associated domain.

(C) Peptide scanning analysis confirms the location of the three Atg8-intertacting motifs (AIM). A membrane-bound array of 176 overlapping peptides of 15 aa, with an offset of 1 aa, covering the entire C-terminal sequence of Ede1, was analyzed for binding to GST-Atg8 by immunoblotting with GST-specific antibodies. As control the same array was synthesized with the important aa in the respective AIM replaced by alanine.

(D) The binding between Ede1 and Atg8 is mainly mediated by AIM2 and 3 *in vitro*. Ni-pulldown assays were used to enrich for Ede1-Atg8 complexes, after recombinant His-tagged Atg8 (His-Atg8, 8 nM) was incubated with different double AIM mutants of GST-tagged Ede1 (Ede1^{AIM1+2}, Ede1^{AIM1+3} or Ede1^{AIM2+3}; 0.8 nM each). Graph shows position of mutants used to map the AIMs. UBA: ubiquitin-associated domain.

(E) Ede1 (1220-1247) peptide renders extended interactions with Atg8 additional to AIM binding. The acidic sidechains of Ede1 pre-AIM sequences form massive polar bonds with the sidechains in the Atg8 N-terminal helix (left). Ede1 post-AIM residues also contribute additional polar contacts to Atg8 (right).

(F) The binding pattern of Ede1 peptide to Atg8 resembles that of ankyrin-derived peptides to Atg8 homologs in mouse (Li et al., 2018). To show an example, a complex of HsAnkB-MsLC3B (PDB No. 5YIS) is superimposed to Ede1-Atg8 (conducted in PyMOL).

(G) ITC results for Atg8 with a peptide of Ede1 (1220-1247) showing that Ede1^{AIM1,2} can bind to Atg8 with micromolar affinities.

(H) Atg8-lipidation is unaffected in *ede1*^{AIMR} mutant cells. Genome replacement of the *EDE1* locus by *ede1*^{AIMR} does not affect Atg8-lipidation as monitored by immunoblotting against Atg8 in wildtype (WT), *ede1*^{AIMR} or Atg7-deficient (*atg7*Δ) cells after addition of 100 nM rapamycin for different durations. Six biologically independent experiments are quantified and the mean ± SD is shown. Pgk1 serves as loading control.

(I) Vacuolar degradation of EGFP-Atg8 is unaffected in *ede1*^{AIMR} mutant cells. N-terminally EGFP-tagged Atg8 under the *ADH* promoter was checked for its autophagic degradation by GFP-cleavage assay in wildtype (WT), *ede1*^{AIMR} and Atg7-deficient (*atg7*Δ) cells following nitrogen starvation in SD-N medium at different times points (3 and 6 hours) at 30 °C. Pgk1 serves as loading control.

(J) Bulk autophagy is not affected in *ede1*^{AIMR} mutant cells. Wildtype (WT), *ede1*^{AIMR}, Ede1-deficient (*ede1*Δ) and Atg7-deficient (*atg7*Δ) cells were grown to mid-log phase in YPD, and then incubated in SD-N for 3 or 6 hours. Samples were analyzed by the Pho8Δ60 assay (Noda and Klionsky, 2008). The average of four independent experiments is quantified and the mean ± SD is shown.

(K) Mitophagy is not impaired in *ede1*^{AIMR} mutant cells. Mitophagy was monitored by EGFP-tagging of Idh1 in wildtype (WT), *ede1*^{AIMR}, and Atg8-deficient (*atg8*Δ) cells, followed by immunoblotting

against EGFP before and after induction of mitophagy in YPG medium (YP-glycerol) for the indicated time. Pgk1 serves as loading control.

(L) Targeting of the Cvt cargo protein Ape1 to the vacuole is not affected in *ede1*^{AIMR} mutant cells. Ape1 processing in the vacuole, i.e. pre-Ape1 (preApe1) to mature Ape1 (mApe1), is monitored before and after addition of 100 nM rapamycin for the indicated time in wildtype (WT), *ede1*^{AIMR}, Atg1-deficient (*atg1*Δ) and Atg19-deficient (*atg19*Δ) cells. Cell lysates for each strain were subjected to immunoblotting against Ape1. The average of eight independent experiments is quantified and the mean ± SD is shown. Pgk1 serves as loading control.

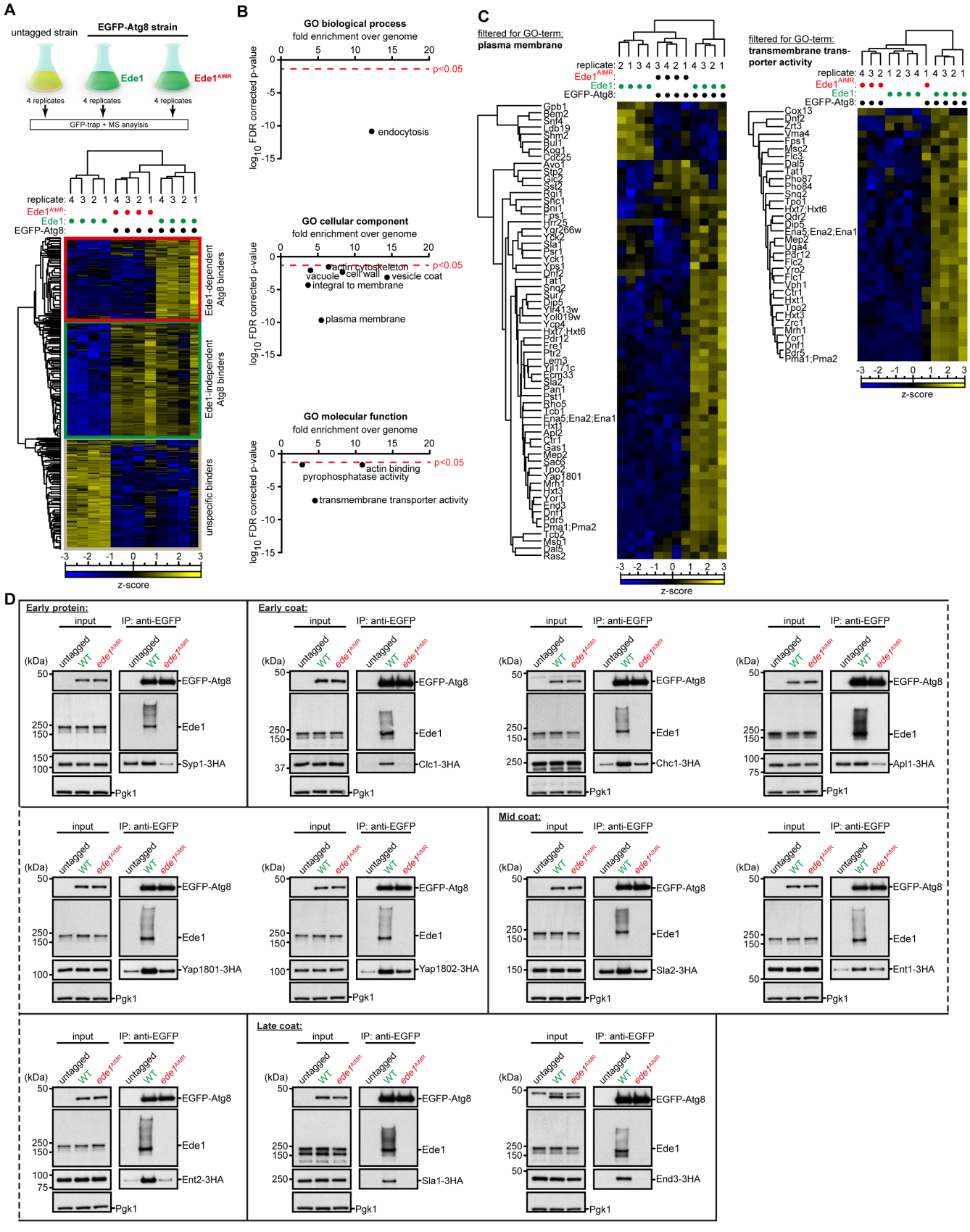
A
untagged strain
EGFP-Atg8 strain
Ede1
Ede1AIMR
4 replicates
4 replicates
4 replicates
GFP-trap + MS anaylsis
replicate: 4 3 2 1 4 3 2 1 4 3 2 1
Ede1AIMR:
Ede1:
EGFP-Atg8:
Ede1-dependent Atg8 binders
Ede1-independent Atg8 binders
unspecific binders
-3 -2 -1 0 1 2 3
z-score
B
GO biological process
fold enrichment over genome
p<0.05
endocytosis
log10 FDR corrected p-value
GO cellular component
fold enrichment over genome
actin cytoskeleton
vacuole
cell wall
vesicle coat
integral to membrane
plasma membrane
GO molecular function
fold enrichment over genome
actin binding
pyrophosphatase activity
transmembrane transporter activity
C
filtered for GO-term:
plasma membrane
Gpb1
Bem2
Snf4
Ldb19
Shm2
Bul1
Kog1
Cdc25
Ayo1
Stp2
Glc7
Sst2
Rgl1
Src1
Bni1
Fps1
Pfk26
Ygr266w
Yck2
Sla1
Psr1
Yck1
Yps3
Dnf2
Tat1
Snq2
Sur7
Dip5
Ylr413w
Yol019w
Ycp4
Hxt7;Hxt6
Pdr12
Fre1
Ptr2
Lem3
Ylr171c
Lcb3
Sla2
Pan1
Pst1
Rho5
Tcb1
Ena5;Ena2;Ena1
Hxt1
Apl2
Ctr1
Gas1
Mep2
Sac6
Ypq2
Yap1801
Mrh1
Hxt3
Yor1
Eng3
Dnf1
Pdr5
Pma1;Pma2
Tcb2
Msb1
Dal5
Ras2
filtered for GO-term:
transmembrane trans-porter activity
Cox13
Dnf2
Zrt3
Vma4
Fps1
Msc2
Plc3
Dal5
Tat1
Pho87
Pho84
Sno2
Tpo1
Hxt7;Hxt6
Qdr2
Dip5
Ena5;Ena2;Ena1
Mep2
Uga4
Pdr12
Flc2
Yro2
Flc1
Vph1
Ctr1
Hxt1
Tpo2
Hxt3
Zrc1
Mrh1
Yor1
Dnf1
Pdr5
Pma1;Pma2
D
Early protein:
Early coat:
Mid coat:
Late coat:
input
IP: anti-EGFP
(kDa)
untagged
WT
ede1AIMR
EGFP-Atg8
Ede1
Syp1-3HA
Clc1-3HA
Chc1-3HA
Apl1-3HA
Yap1801-3HA
Yap1802-3HA
Sla2-3HA
Ent1-3HA
Ent2-3HA
Sla1-3HA
End3-3HA
Pgk1

Figure S3. Ede1 Is an Autophagy Receptor for Endocytic Machinery Proteins, Related to Figure 3

(A) Workflow of EGFP-Atg8 pulldown with subsequent qMS analysis. Four biological replicates of a strain expressing EGFP-Atg8 under the *ADH* promoter with WT Ede1 or mutant Ede1^{AIMR} present as well as four replicates of an untagged wildtype strain were subjected to immunoprecipitation against EGFP after the induction of autophagy with 100 nM rapamycin for 3 hours and analysed by label-free quantitative MS. Shown is the hierarchical clustering of the respective z-scores for ANOVA-positive and FDR corrected hits from each sample. The red box highlights Ede1-dependent Atg8 interactors. The green box highlights Ede1-independent Atg8 interactors and grey box shows unspecific binders.

(B) Clathrin-mediated endocytosis and PM proteins bind Atg8 specifically through Ede1. Gene Ontology GO-term analysis of proteins enriched in the EGFP-Atg8 pulldown that bind in an Ede1-dependent manner. The results for the GO enrichment analysis were obtained by using the GENEONTOLOGY search engine (http://geneontology.org).

(C) Hierarchical cluster analysis of label-free EGFP-Atg8 pulldowns identifies Ede1-dependent Atg8 interactors for GO-term plasma membrane or transmembrane transporter activity. Pulldown and qMS analysis of N-terminally EGFP-tagged Atg8 (p*ADH*) interactors determined from wildtype (WT), *ede1*^{AIMR} or untagged cells. Shown is the hierarchical clustering of the respective z-scores for ANOVA-positive and FDR corrected hits from each sample after filtering proteins significantly enriched for the GO-term (cellular component) plasma membrane (left) or (molecular function) transmembrane transporter activity (right).

(D) Validation of the Ede1 dependent cargo binding to EGFP-Atg8. Ede1-dependent cargo proteins identified by qMS (Syp1, Clc1, Chc1, Apl1, Yap1801, Yap1802, Sla2, Ent1, Ent2, Sla1 and End3) were C-terminal tagged with 3HA in wildtype (WT) and *ede1*^{AIMR} mutant cells and checked for their binding to EGFP-Atg8 by co-immunoprecipitation using GFP-trap beads. Binding of Ede1 to EGFP-Atg8 was monitored by immunoblotting with an antibody against Ede1. A strain without the EGFP-tagged Atg8 served as control. Pgk1 serves as loading control for the input.

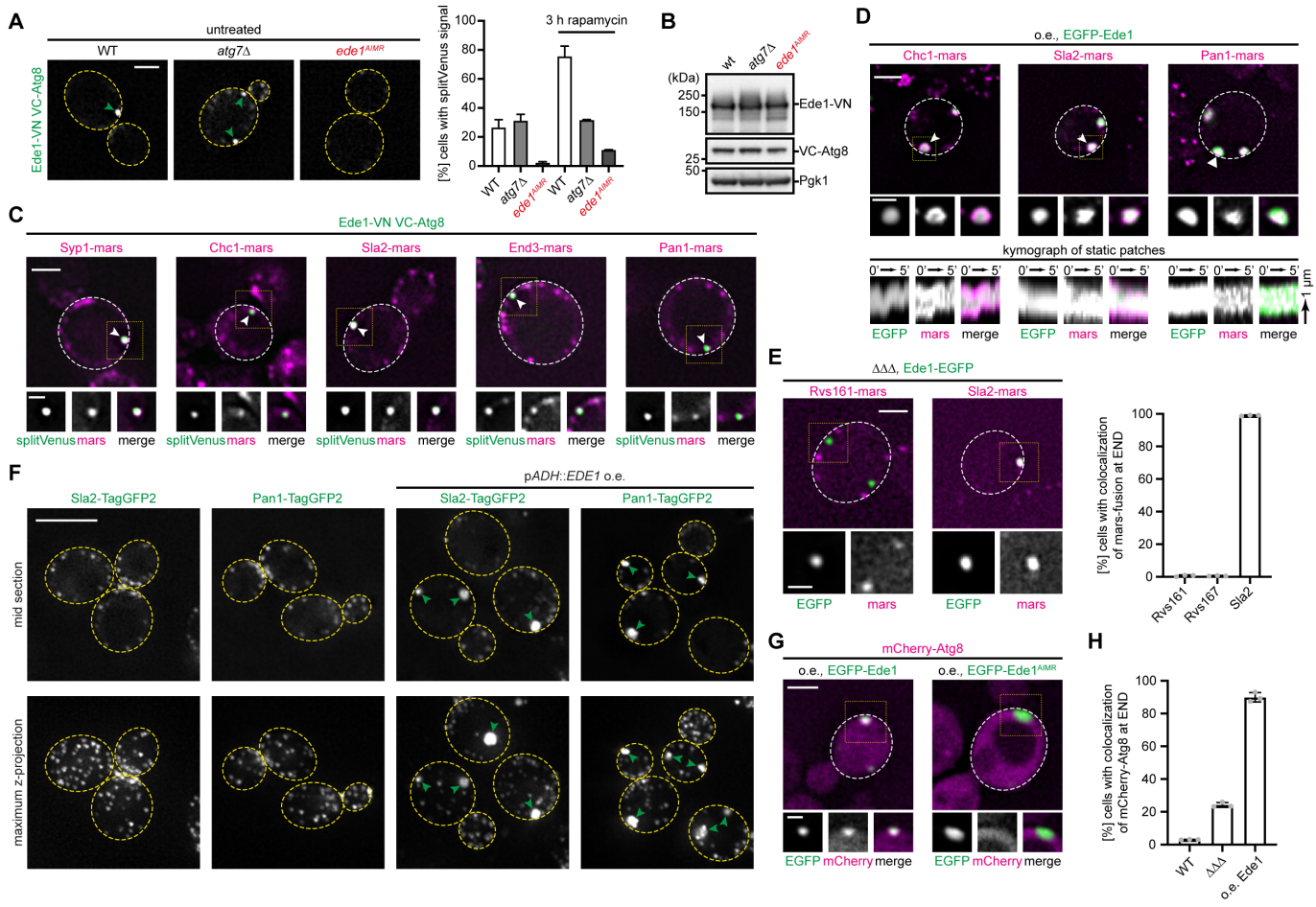

Figure S4. CME Proteins Accumulate in END, Related to Figure 3

(A) Ede1 interacts with Atg8 at distinct sites at the cell periphery. Interaction of Ede1 with Atg8 is shown by BiFC fluorescent signal resulting from VC-Atg8 (p*ADH*) and Ede1-VN in WT, *atg7*Δ, or *ede1*^{AIMR} cells. Arrowheads indicate interaction sites at the PM. Quantifications are based on 500 or more cells from two independent experiments and displayed as mean ± SD. Scale bar represents 2 µm.

(B) Protein levels of splitVenus (VN and VC) tagged Ede1 and Atg8 are unchanged in different mutant strains. Immunoblotting against Ede1 and Atg8 with the respective antibodies in WT, Atg7-deficient (*atg7*Δ), or *ede1*^{AIMR} mutant cells.

(C) Endocytic proteins accumulate at sites of Ede1-Atg8 interaction. Different mars-tagged proteins from the endocytic machinery (Syp1 (early protein), Chc1 (early coat), Sla2 (mid coat) and Pan1/End3 (late coat)) colocalize to sites of Ede1-Atg8 interaction marked by the BiFC signal of p*ADH::*VC-*ATG8* and Ede1-VN. Scale bar represents 2 µm and 1 µm for inset.

(D) The CME proteins Chc1, Sla2 and Pan1 stably colocalize at sites of EGFP-Ede1 accumulation. Kymograph representation of a two-color movie (1 frame/20 s) recorded by fluorescence microscopy of cells overexpressing EGFP-Ede1 under the control of the *ADH* promoter and either Chc1-mars, Sla2-mars, or Pan1-mars. Scale bar represents 2 µm or 1 µm for inlets and kymographs.

(E) Rvs161 and Rvs167 important for the scission of the clathrin coated vesicle are excluded from sites of aberrant Ede1 clustering. Colocalization experiments between Rvs161- or Rvs167-mars and Ede1-EGFP in the ΔΔΔ strain background. Lower panels show magnifications of boxed areas. Scale bar represents 2 µm and 1 µm for inset. Quantifications are based on 200 or more cells from n = 3 independent experiments and displayed as mean ± SD.

(F) Stable accumulation of CME proteins is independent of the EGFP-tag. Sla2 and Pan1 where endogenously tagged with the monomeric fluorescent protein TagGFP2 in cells where Ede1 expression was either controlled by the endogenous or the *ADH* promoter. Green arrows indicate sites of CME protein accumulation. Scale bar represents 5 µm.

(G) Atg8 colocalizes AIM-dependent with EGFP-Ede1 clusters in Ede1 overexpressing cells. Colocalization experiments between mCherry-Atg8 (p*ADH*) and EGFP-Ede1 or EGFP-Ede1^{AIMR} (p*ADH*). Lower panels show magnifications of boxed areas. Scale bar represents 2 µm and 1 µm for inset.

(H) Quantification of the percentage of cells showing colocalization of EGFP-tagged Ede1 and mCherry-Atg8 (*pADH*) in WT, ΔΔΔ and Ede1 overexpressing cells. Quantifications are based on 200 or more cells from three independent experiments and displayed as mean ± SD.

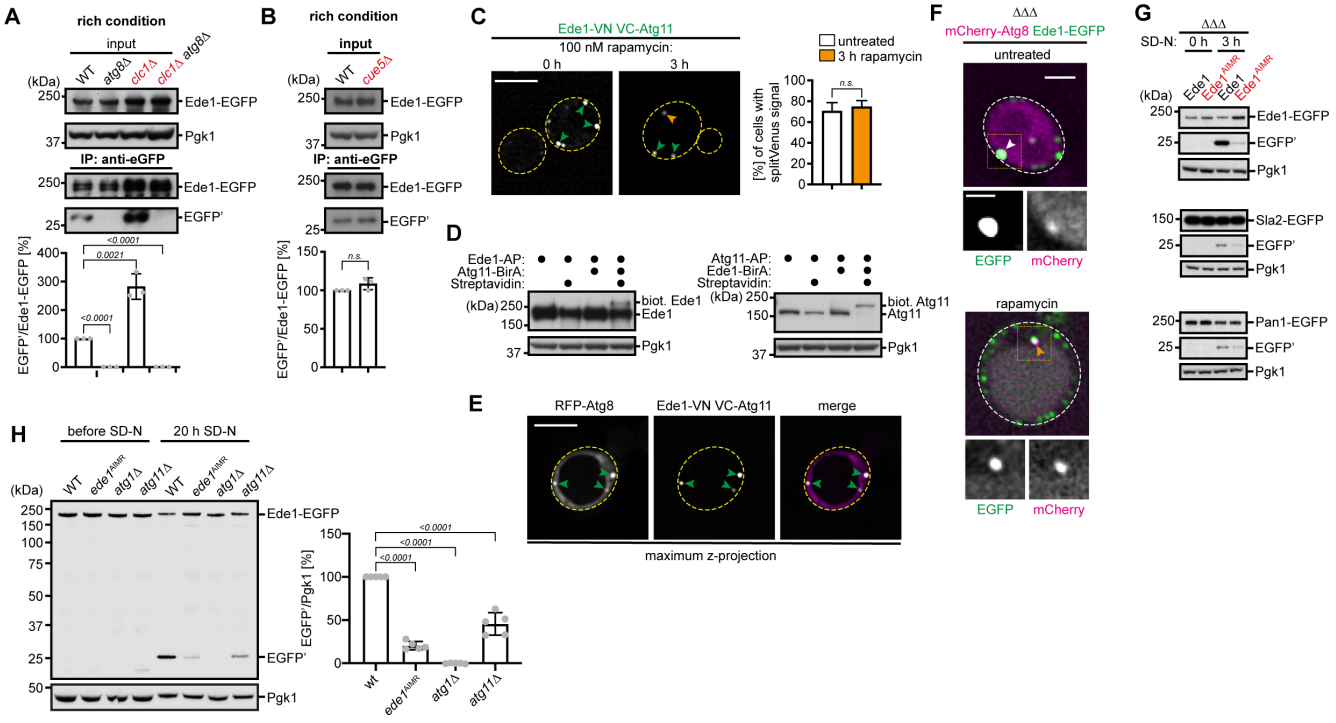

Figure S5. Involvement of Atg11 Scaffold in Autophagic END Degradation, Related to Figure 4

(A-B) Autophagic turnover of Ede1 is detected during logarithmic growth in WT and enhanced in *clc1*Δ mutant cells (A) but unaffected in *cue5*Δ (B). EGFP pulldowns were performed in WT, *clc1*Δ or *cue5*Δ mutant cells expressing endogenously EGFP-tagged Ede1. The pulldown of vacuolar enriched free EGFP from WT, *clc1*Δ or *cue5*Δ mutant was compared to cells additionally deficient in the core autophagy protein Atg8 (*atg8*Δ). A quantification of the ratio between free EGFP' and full length Ede1-EGFP is shown. Data are mean ± SD of n = 3 biologically independent experiments. Statistical analysis was performed using two-tailed Student's *t*-tests, *p*-values are indicated. Pgk1 serves as input control.

(C) Ede1 interacts with Atg11 at similar sites as seen for Atg8. Interaction of Ede1 with Atg11 is shown by BiFC fluorescent signal resulting from VC-Atg11 (p*ADH*) and Ede1-VN before and after a 3 h treatment with 100 nM rapamycin. Green arrowheads indicate interaction sites at the END, whereas orange arrowheads indicate interaction sites at the PAS. Quantifications are based on 500 or more cells from two independent experiments and displayed as mean ± SD. Scale bar represents 5 µm.

(D) Site-specific biotinylation assays identify interaction between Ede1 and the autophagic scaffold protein Atg11. Tagging of Ede1 or Atg11 with the biotin ligase BirA leads to biotinylation of the respective other protein tagged with a combination of a TAP-tag and an acceptor peptide (AP). After addition of Streptavidin upshifted protein bands were detected by immunoblotting with peroxidase anti peroxidase (PAP) antibody.

(E) RFP-Atg8 colocalizes to sites of Ede1-Atg11 interaction. Cells expressing VC-Atg11 (p*ADH*) and Ede1-VN accumulate RFP-Atg8 at sites of BiFC signal. Arrowheads indicate interaction sites at the END. Scale bar represents 5 µm.

(F) Ede1-EGFP is targeted to the vacuole upon rapamycin treatment. Recruitment of Atg8 to sites of Ede1 accumulation is visualized by colocalization of mCherry-Atg8 (p*ADH*) and Ede1-EGFP in the ΔΔΔ strain background before and after 100 nM rapamycin treatment for 3 hours. Arrow on the top image shows colocalization at sides of Ede1 clustering. Arrow on the bottom image shows colocalization at the PAS. Lower panels show magnifications of boxed areas. Scale bar represents 2 µm and 1 µm for inset.

(G) END accumulated Sla2 and Pan1 are degraded by autophagy upon nitrogen starvation. The mid coat protein Sla2 or the late coat protein Pan1 were C-terminally EGFP-tagged in WT or ΔΔΔ (*yap1801*Δ, *yap1802*Δ, *apl3*Δ) cells with endogenous expression of Ede1 or Ede1^{AIMR}, and its starvation-induced autophagic processing was analyzed by GFP-cleavage assay. Top shows degradation of Ede1-EGFP or Ede1^{AIMR}-EGFP under the same conditions.

(H) Atg11 is only partially important for autophagic degradation of Ede1 under bulk conditions. Endogenous Ede1 was C-terminally EGFP-tagged in WT, Ede1^{AIMR}-mutated (*ede1*^{AIMR}), Atg1-deficient (*atg1*Δ) or Atg11-deficient (*atg11*Δ) cells, and its starvation-induced autophagic degradation was analyzed by GFP-cleavage assay. EGFP′ is EGFP-fragment generated by Ede1-EGFP degradation in the vacuole. Data are mean ± SD of n = 5 biologically independent experiments. Statistical analysis was performed using two-tailed Student's *t*-tests, *p*-values are indicated. Pgk1 serves as input control.

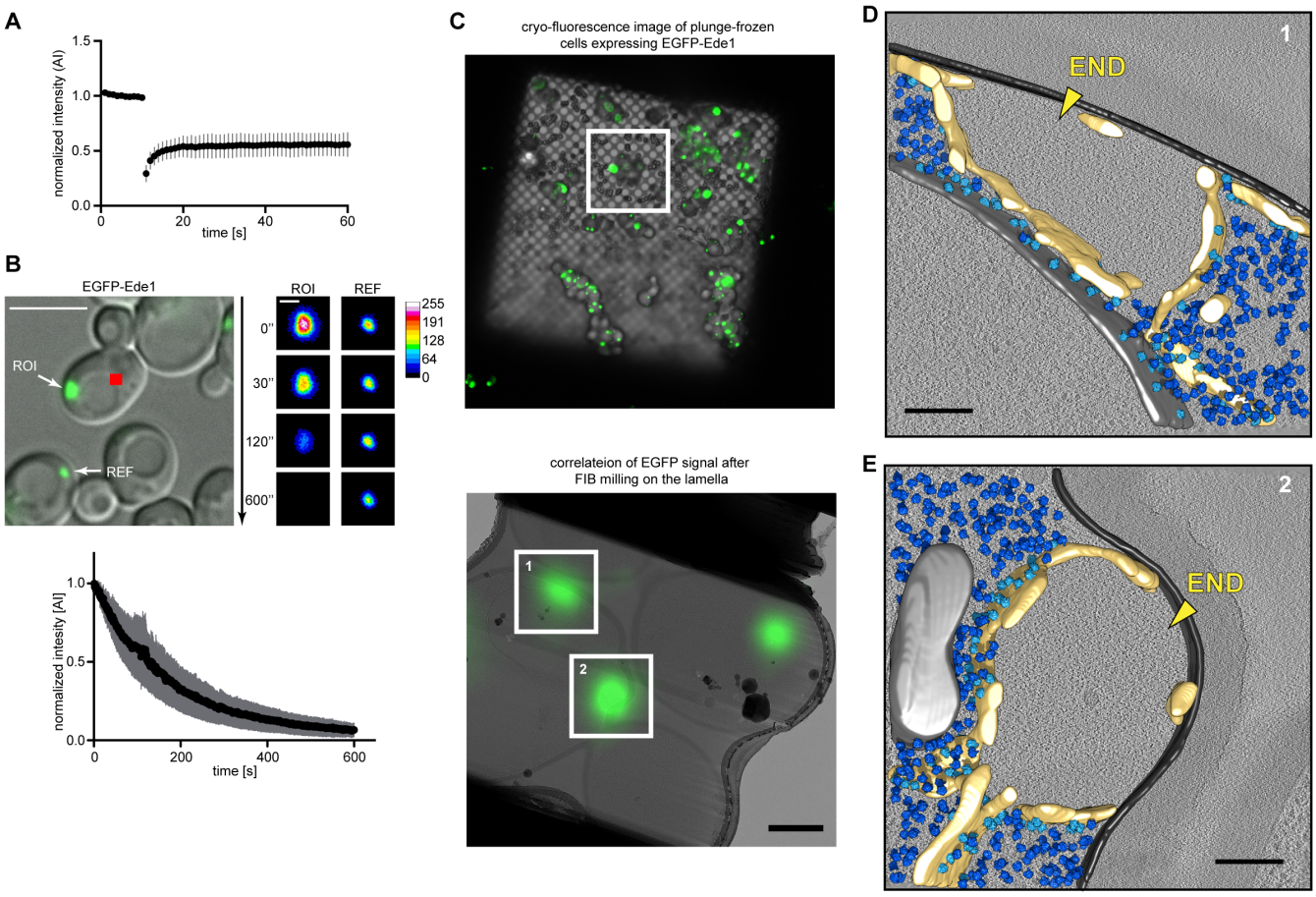

Figure S6. Biophysical and Ultrastructural Dissection of END, Related to Figure 5

(A) Single normalization analysis of FRAP data shown in Figure 5A.

(B) EGFP-Ede1 adjacent to the PM can readily exchange with the cytosol. Fluorescence loss in photobleaching (FLIP) experiments were performed for cells overexpressing EGFP-Ede1 under the control of the *ADH* promoter. The indicated spot (red) is bleached after each image for a time course of 600 s and the fluorescence within the region of interest (ROI) is measured. As reference for bleaching effects serves the END of a neighboring cell (REF). Representative images of one experiment are shown. Quantification shows the loss of EGFP-Ede1 signal over time from at least three independent experiments as mean ± SD. Scale bar represents 5 µm and 1 µm for inset. n = 4 biologically independent experiments.

(C-E) Ultrastructural dissection of the Ede1 accumulations in the overexpression strain by 3D-correlated cryo-light and cryo-electron microscopy (cryo-CLEM). After cryopreservation, potential sites of interest are located by fluorescence light microscopy (FLM) ((C), top image) and scanning electron microscopy (SEM). Correlative beads are both located in FLM and the ion beam (IB) mode of a dual beam focused ion beam (FIB) SEM to obtain a 3D correlation between both imaging modes. Predicted points of interests are then calculated from the FLM 3D stack data, promising sites are selected and cut using the cryo-FIB resulting in thin lamellas. Finally, 2D correlation can be performed between beads in the FLM and transmission electron microscope (cryo-TEM) images to obtain points of interest on the lamellas ((C), bottom image), which are then analyzed in detail by

high-resolution cryo-TEM (cryo-CLEM). In this example, two tomograms are recorded at the sites of correlated signal ((C) bottom image 1 and 2, corresponding to D and E), reconstructed and segmented. Both examples (D and E) show areas of Ede1 protein accumulations, which are surrounded by endoplasmic reticulum. The interior of the amorphous protein structure is clearly devoid of all ribosomes (light and dark blue) and originates directly from the plasma membrane (light grey). Membrane-associated ribosomes (light blue) are exclusively found on parts of the ER facing the cytosol. Other organelles in the vicinity, such as the nuclear membrane (light grey, D) or mitochondria (light grey, E), appear unchanged. The scale bar in (C, top) represents 20 μm, in (C, bottom) 1 μm and (D and E) 200 nm.

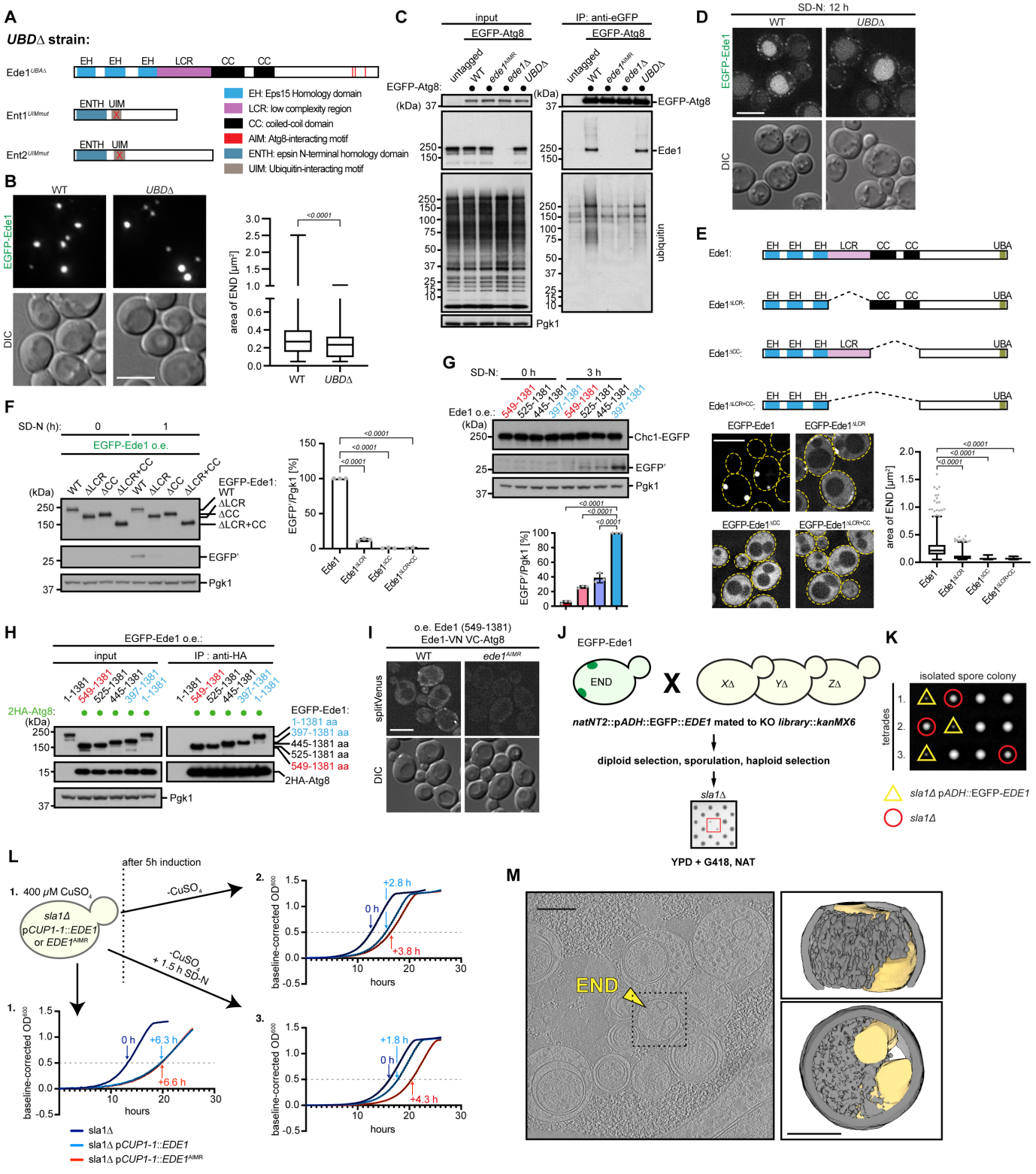

Figure S7. Phase-Separation of Ede1 but Not Ubiquitin Binding Is Important for Autophagic Degradation, Related to Figure 6 and 7

(A-B) Ubiquitin binding motifs within endocytic machinery proteins are dispensable for END formation. Illustration shows mutants used to create the *UBD*Δ strain (A). EH: Eps15-homology domain; LCR: low complexity region; CC: coiled-coil domain; UBA: ubiquitin-associated domain; ENTH: epsin N-terminal homology domain; UIM: Ubiquitin-interacting motif. END formation driven by expression of Ede1 under the control of the *ADH* promoter is monitored by fluorescence microscopy of WT and *UBD*Δ (deletion of the UBA domain of Ede1, and mutation of both UIMs in Ent1 and Ent2) mutant cells (B). Spots size was analyzed computational from maximum z-projections of the corresponding strains for a total of more than 3000 spots of n = 6 biologically independent experiments.

(C) Ede1-Atg8 interaction is unaffected in *UBD*Δ cells but binding of ubiquitylated cargo proteins is decreased. Atg8 expressed under the *ADH* promoter was EGFP-tagged, and its interaction with Ede1 was probed by co-immunoprecipitation and immunoblotting with the respective antibodies in WT, *ede1*^{AIMR}, *ede1*Δ, or *UBD*Δ cells. Pgk1 was used as loading control for the input.

(D) Autophagic turnover of Ede1 in *UBD*Δ cells is unaffected. Cells expressing EGFP-Ede1 (p*ADH*) in WT or *UBD*Δ cells were starved for 12 hours in medium lacking nitrogen before monitored by fluorescence microscopy.

(E) END formation depends on the Ede1 LCR and coiled coil domain. The different Ede1 mutants were expressed under the *ADH* promoter and formation of the END was monitored by fluorescence microscopy of the EGFP-Ede1 signal. Spots size was analyzed computational from maximum z-projections of the corresponding strains for a total of more than 500 spots of n = 3 biologically independent experiments. Statistical analysis was performed using two-tailed Student's *t*-tests, *p*-values are indicated. Illustration shows deletion mutants used to map the region important to undergo phase-separation. EH: Eps15-homology domain; LCR: low complexity region; CC: coiled-coil domain; UBA: ubiquitin-associated domain; aa: amino acid. Scale bar represents 5 µm.

(F) Autophagic degradation of Ede1 depends on its LCR and coiled coil domain. Mutants expressing N-terminal EGFP-Ede1 (*pADH*) deleted for the LCR (ΔLCR), coiled coil (ΔCC) or both at the same time (ΔLCR+CC) were analyzed by GFP-cleavage assay before and after 1 hour of nitrogen starvation. Quantifications of free EGFP' levels normalized to Pgk1 are shown. Pgk1 serves as a loading control. Data are mean ± SD of n = 3 biologically independent experiments. Statistical analysis was performed using two-tailed Student's *t*-tests, *p*-values are indicated.

(G) LCR of Ede1 is necessary for autophagic degradation of the Ede1-dependent substrate Chc1. Cells in which Chc1 was endogenously EGFP-tagged and co-expressing different N-terminal Ede1 truncation mutants from the *ADH* promoter were analyzed by GFP-cleavage assay before and after 3 h of nitrogen starvation. Quantifications of free EGFP' levels normalized to Pgk1 are shown. Data are mean ± SD of n = 3 biologically independent experiments. Statistical analysis was performed using two-tailed Student's *t*-tests, *p*-values are indicated.

(H-I) Ede1 binding to Atg8 is independent of the presence of the LCR. Atg8 expressed under the *ADH* promoter was 2HA-epitope-tagged, and its interaction with different N-terminal EGFP-tagged Ede1 truncation mutants (under the *ADH* promoter) was probed by co-immunoprecipitation and immunoblotting with anti-GFP antibody (H). Also, an AIM dependent BiFC signal for Ede1$^{549-1381}$-VN and VC-Atg8 both expressed under the *ADH* promoter is observed by fluorescence microscopy (I).

(J) Scheme of the robot-based synthetic lethal screen, which identified the strong synthetic interaction between overexpression of Ede1 and Sla1. A library of nonessential gene deletions (all G418 resistant) was mated with a bait strain overexpressing Ede1 from the *ADH* promoter (NAT resistant). Diploid cells were selected and subjected to sporulation. Finally, haploid cells were selected by pinning on YPD plates containing both selection markers G418 and NAT.

(K) Manual crossing of a *sla1*Δ with the EGFP-Ede1 overexpression strain followed by tetrad dissection confirms the screening results.

(L) The Ede1 AIM-binding mutant causes delayed growth in sla1Δ mutant cells. Growth curves for cells deficient in Sla1 (*sla1*Δ) and cells deficient in Sla1 (*sla1*Δ) overexpressing either EGFP-Ede1 or EGFP-Ede1^{AIMR} were measured: 1.) in YPD medium under constant Ede1 expression (400 µM $CuSO_4$); 2.) in YPD medium without $CuSO_4$ (Ede1 repression); or 3.) treated for 1.5 h with medium lacking nitrogen prior to measuring the growth curve in YPD medium without $CuSO_4$. Growth curves are displayed as average for n = 3 individual experiments. The time difference reaching OD 0.5 for *sla1*Δ overexpressing either EGFP-Ede1 or EGFP-Ede1^{AIMR} are compared to *sla1*Δ alone.

(M) The END accumulates exclusively in autophagic bodies under rich growth conditions. Ultra-structural analysis of ΔΔΔ cells expressing Ede1-EGFP (endogenous locus) by cryo-ET in Atg15-deficient (*atg15*Δ) and Atg19-deficient (*atg19*Δ) cells after entering stationary phase (OD 5). The example shows Ede1-EGFP protein accumulation together with fenestrated ER within autophagic bodies inside the vacuole. Shown is an average 2D section of the original tomogram (left). Scale bar represents 200 nm. Segmentation shows top and side view of the END containing autophagic body. The autophagic body membrane is shown in light grey; drop-like protein accumulations are indicated in dark grey (by a density threshold) and membranes surrounding the protein accumulation are segmented in light yellow. Scale bar represents 200 nm and 100 nm for inset.

SUPPLEMENTAL TABLES

Table S1. Gene Knockouts That Stabilize the END Compartment Upon Nitrogen Starvation, Related to Figure 4G.

Systematic Name:	Standard Name:	z-score (number of spots/area)	z-score (number of spots/area)
		basal	**after starvation**
YDL077C	VAM6	0.95	10.10
YLL042C	ATG10	-0.55	10.09
YDL149W	ATG9	-0.14	9.96
YBR128C	ATG14	-0.02	9.92
YBR217W	ATG12	0.63	9.72
YMR159C	ATG16	-0.07	9.69
YPL149W	ATG5	-0.14	9.55
YMR158W-A	-	0.34	9.48
YML001W	YPT7	-0.07	9.07
YNR007C	ATG3	0.54	9.06
YJL036W	SNX4	0.27	8.97
YPL120W	VPS30	0.52	8.91
YNL242W	ATG2	0.50	8.86
YBR131W	CCZ1	0.60	8.77
YBL078C	ATG8	-0.35	8.29
YGL212W	VAM7	1.01	7.84
YDL113C	ATG20	0.84	7.82
YOL004W	SIN3	1.80	7.61
YBL089W	AVT5	-0.16	7.48
YOR106W	VAM3	0.79	7.30
YDR080W	VPS41	1.01	7.30
YCR032W	BPH1	-0.05	7.19
YNL223W	ATG4	n.a.	7.16
YFR021W	ATG18	-0.04	7.13
YEL013W	VAC8	-0.70	7.12
YGL180W	ATG1	0.85	7.03
YGR159C	NSR1	0.03	6.86
YHR171W	ATG7	0.37	6.46
YDR108W	TRS85	0.25	5.98
YGR064W	-	-0.53	5.31
YBL072C	RPS8A	n.a.	5.30
YKR001C	VPS1	1.98	5.27
YNR006W	VPS27	0.50	5.21
YDR079C-A	TFB5	-0.30	5.18
YNL097C	PHO23	1.12	5.14
YPR185W	ATG13	0.16	5.04
YML010W-A	-	0.28	4.82
YMR263W	SAP30	1.50	4.73
YPL002C	SNF8	0.09	4.65
YJR073C	OPI3	0.77	4.56
YPR173C	VPS4	0.70	4.28
YLR423C	ATG17	-0.06	4.21
YJL124C	LSM1	-0.73	4.03
YLR148W	PEP3	0.99	3.97
YCR068W	ATG15	0.10	3.94

YEL062W	NPR2	0.12	3.83
YPL139C	UME1	0.66	3.83
YER014C-A	BUD25	-0.15	3.52
YHR025W	THR1	0.51	3.44
YNL296W	-	0.42	3.36
YAL013W	DEP1	0.77	3.24
YHR004C	NEM1	0.33	3.20
YLR431C	ATG23	0.52	3.11
YDL047W	SIT4	-0.21	3.08
YGL035C	MIG1	-0.15	2.99
YOL081W	IRA2	-0.63	2.95
YER161C	SPT2	0.86	2.95
YLR119W	SRN2	0.27	2.80
YBR251W	MRPS5	n.a.	2.78
YNL136W	EAF7	-0.18	2.62
YDR225W	HTA1	-0.23	2.60
YHL023C	NPR3	n.a.	2.58
YNL213C	RRG9	-2.11	2.58
YCL008C	STP22	1.09	2.53
YIL125W	KGD1	0.48	2.53
YKL155C	RSM22	0.25	2.46
YGL148W	ARO2	0.90	2.43
YKL002W	DID4	0.39	2.43
YGL244W	RTF1	-0.21	2.36
YGR240C	PFK1	0.41	2.35
YJL006C	CTK2	0.56	2.32
YDR017C	KCS1	0.45	2.32
YJL169W	-	0.40	2.32
YHR082C	KSP1	-0.60	2.21
YPL230W	USV1	1.50	2.19
YKL053C-A	MDM35	0.04	2.17
YBL042C	FUI1	-0.16	2.10
YDR074W	TPS2	0.75	2.07
YPL180W	TCO89	-0.07	1.99
YPL097W	MSY1	0.46	1.94
YGR223C	HSV2	0.68	1.94
YIR009W	MSL1	0.23	1.92
YML014W	TRM9	-0.66	1.90
YGR270W	YTA7	-0.26	1.86
YML073C	RPL6A	1.29	1.84
YDR207C	UME6	-0.87	1.82
YNR010W	CSE2	0.78	1.81
YPL100W	ATG21	0.03	1.79
YNL215W	IES2	n.a.	1.75
YBR126C	TPS1	0.73	1.72
YMR179W	SPT21	0.56	1.69
YDR149C	-	-0.15	1.68
YGR184C	UBR1	0.03	1.68
YKL146W	AVT3	-0.93	1.66
YHR192W	LNP1	-0.47	1.63
YOR141C	ARP8	-0.43	1.61
YPR051W	MAK3	0.21	1.60
YNL224C	SQS1	-1.08	1.55

YPR070W	MED1	0.27	1.55
YPR133W-A	TOM5	1.05	1.54